Thermal shielding performance of self-healing hydrogel in tumor thermal ablation

Lifei Huang [a],[1], Shiyuan Yang [b],[1], Mingyu Bai [b], Yuxuan Lin [b], Xue Chen [a], Guofeng Li [a], Li-gang Cui [b],[*], Xing Wang [a],[*]

[a] Beijing Laboratory of Biomedical Materials, Beijing University of Chemical Technology, Beijing 100029, PR China
[b] Department of Ultrasound, Peking University Third Hospital, Beijing 100191, PR China

ARTICLE INFO

ABSTRACT

Thermal ablation therapy is widely used in the surgical treatment of tumors. Clinically, normal saline is generally used as an insulator to protect adjacent tissues from local high-temperature burns caused by thermal ablation. However, the flow of saline causes fluid loss, requiring frequent injections and complex operation, which is easy to lead to complications such as secondary injury and hematoma. Here, a self-healing chitosan-PEG (CP) hydrogel was proposed as a protective medium to challenge the clinical preparations. Compared with saline and non-self-healing hydrogel F127, CP hydrogel exhibited outstanding thermal shielding performance in the thermal ablation of thyroid nodule in a Beagle dog model. The transient plane source (TPS) method is used to measure thermal properties, including thermal conductivity, thermal diffusivity and specific heat capacity. The thermal shielding mechanism and clinical advantages including operability, biodegradability, and biological safety of self-healing hydrogel are then revealed in-depth. Therefore, self-healing hydrogel can achieve much better thermal management in tumor thermal ablation.

1. Introduction

Thermal ablation as an important tumor treatment method is developing rapidly due to its outstanding advantages of minimally invasion, fast and accurate, low pain and high efficiency [1–5]. Thermal ablation techniques such as microwave, laser and radiofrequency have been widely used in the treatment of various benign and malignant tumors, including tumor diseases at thyroid, breast, uterus, liver, lung, kidney and prostate [6–10]. Klapperich et al. achieved 100% technical success in the subcutaneous microwave ablation (MWA) treatment of 100 cases of T1a stage renal cell carcinoma [11]. However, the local high temperature produced by thermal ablation might damage the adjacent tissues, leading to the emergence of multiple complications [11–13]. Izzo et al. reported a postoperative complication rate of 5% by employing MWA for primary liver tumors [12]. Maduka et al. identified 6817 patients after thermal ablation of the benign thyroid nodule, displaying 2.0% neck hematoma and 5.2% recurrent laryngeal nerve injury [13]. Clinically, although normal saline has been used as insulator to isolate the tumor from adjacent tissues to prevent the local burns

generated by ablation [14–19], its leachability and thermal conductivity greatly increase the risk of tissues thermal injury and complications [13, 20–22].

Hydrogel is a widely used biomaterial with high water absorbency, water preservation and shapeability [23–25]. In the percutaneous radiofrequency ablation, Wang et al. used the thermal sensitive hydrogel as insulator to separate the gut from the ablation zone of the renal tumor to reduce the intestinal injury [26]. In previous works, a chitosan-based hydrogel based on Schiff base exhibited excellent utility in the basis of properties of self-healing [27], injectability [28], and biocompatibility [29]. The dynamic Schiff base endows it a feature of "flowing solid" [30], thereby contributing to a spatiotemporal dynamic therapy for orderly tissue regeneration [31]. Moreover, polyethylene glycol (PEG) is known as a typical organic phase change material with large heat capacity and high thermal stability [32,33]. Therefore, all these characteristics indicate that this kind of self-healing hydrogels has potential application as a protective medium for thermal ablation of tumors.

Here, we prepared a self-healing chitosan-PEG (CP) hydrogel by adding polymers, glycol chitosan and dual-functionalized PEG (DF-

---

PEG), directly into liquid normal saline (Scheme 1). The dynamic CP hydrogel can be injected into the isolation region and adapt to the irregular tissue lumen, resulting in an entire hydrogel shield to protect adjacent tissues. Compared with liquid saline, CP hydrogel has saline retention and formability which may cause better thermal shielding effectiveness. Considering the clinical usage of thermosensitive F127 hydrogel, the self-healing feature of CP hydrogel is superior to non-healing F127 hydrogel, since for F127 hydrogel, (i) temperature dependence increases the difficulty of operation, (ii) non-healing leads to uneven medium and (iii) the well-known gelling property requires high solid content. In order to test the hypothesis above, their performances were investigated in MWA of thyroid nodule in the Beagle dog model. Through the comparative study of three experimental groups (saline, F127 and CP), the advantages of self-healing CP hydrogel were demonstrated. The mechanism was then revealed based on the in-depth analysis of their thermal properties. We believe that self-healing hydrogel plays a crucial role in the thermal management of clinical tumor thermal ablation.

2. Materials and methods

2.1. Materials

Glycol chitosan (GC, 82 kDa, 85% degree of deacetylation) was purchased from Wako Pure Chemical Industries, Ltd, Japan. DF-PEG (Mn ≈ 4000 g/mol) was synthesized according to the steps in the previous article [30]. Pluronic®F127 (> 98%) was purchased from Beijing Kehua Jingwei Technology Co., Ltd. RPMI 1640 medium (RPMI 1640), penicillin-streptomycin (PS), fetal bovine serum (FBS), and trypsin were purchased from Gibco Life Technologies (Beijing, China). The mouse fibroblast cells (L929) were acquired from Cell Resource Center, IBMS, CAMS/PUMC (Beijing, China). Beagle dogs were obtained from Beijing Marshall Biotechnology Co., Ltd. All Beagle dogs were kept in the animal room of Peking University Third Hospital. All experimental animal protocols were carried out following Beijing (China) Animal Experiment Guidelines (2010) and were authorized by the ethics committee of Peking University Third Hospital (Approve number: 2021-005-02). All

solvents were purchased from Sinopharm Chemical Reagent and used directly without further purification.

2.2. Preparation and characterization of CP hydrogel

3 wt% GC solution and 1 wt% DF-PEG solution were prepared by dissolving GC and DF-PEG in normal saline, respectively. Then, DF-PEG solution and GC solution were mixed evenly at a volume ratio of 3:1 to obtain 2.5% CP hydrogel (2.5% CPH). F127 is widely used for thermal-sensitive hydrogel. 2.5%, 16% and 20% F127 were prepared by dissolving a certain amount of F127 in normal saline. The mechanical strength of 2.5% CPH was performed using an AR-G2 rheometer (TA Instruments, USA) with parallel plate geometry (20 mm diameter). In rheological analysis, the "oscillation frequency" sweep mode was used. The temperature was 25 °C. The strain was 1% and the angular frequency was from 0.1 to 100 rad/s. The experiment was repeated three times. After 2.5% CPH was freeze-dried, it was glued on the conductive glue and sprayed with gold. The microstructure of the hydrogel was characterized by SEM (JEOL JSM-7800 F, JEOL, Japan). The acceleration voltage used for the SEM analysis was 10.0 kV.

2.3. Self-healing property

The self-healing process is qualitatively monitored by rheological analysis. Briefly, the amplitude oscillatory force was changed from $\gamma = 1$–1000% at the same frequency (1.0 Hz) to test the mechanical performance recovery of the hydrogel. The process was repeated three times. Then a disc-shaped CP hydrogel was prepared and cut into two equal parts. One with a trace of methylene blue and the other with a trace of orange. Two semicircular hydrogels of different colors were placed together. Photographs were taken at different intervals to record the healing process.

2.4. Self-adapting property

In this test, 2.5% CPH was injected into a glass bottle by using a No. 22 syringe and a trace of methylene blue was added on the top of
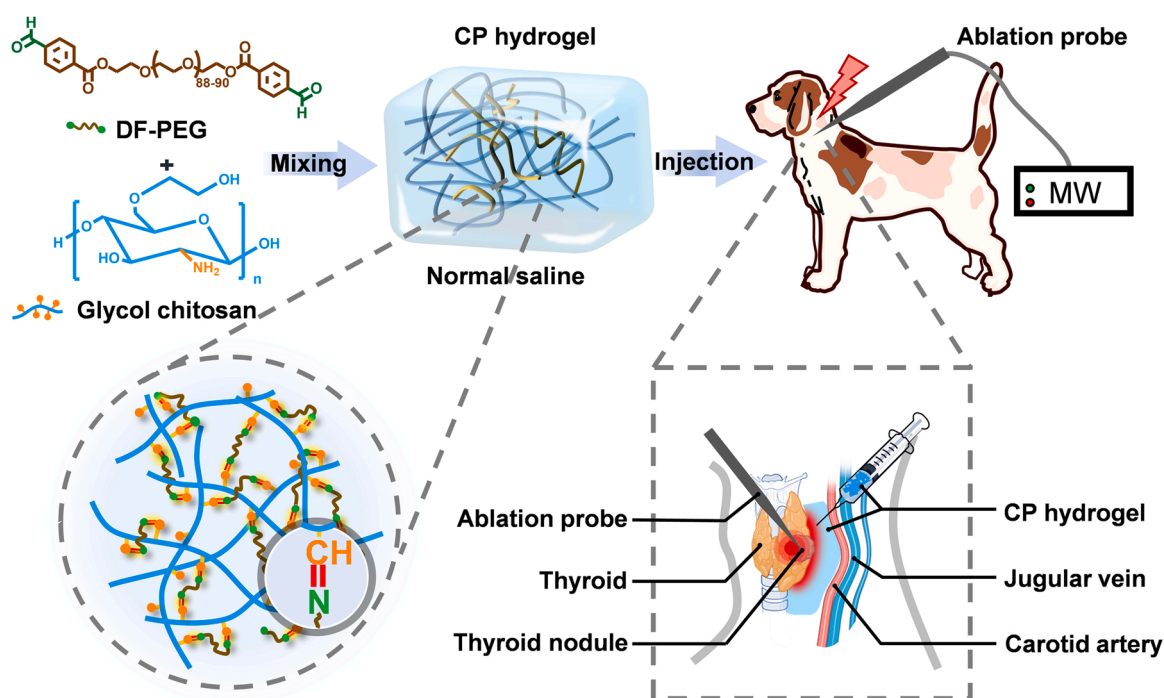
Scheme 1. Schematic illustration of the injectable self-healing CP hydrogel used for a typical MWA treatment of thyroid nodule in the Beagle dog model. CP hydrogel is formed with glycol chitosan and dual-functionalized PEG (DF-PEG).

hydrogel. To demonstrate the shape adaptability of CP hydrogel, 20% F127 was used as control. Afterward, the shape of the hydrogel adapting to the shape of the glass bottle under gravity was recorded.

2.5. In vitro three-dimensional (3D) cell culture and biocompatibility

To investigate the biocompatibility, L929 cells were 3D cultured in CP hydrogel to evaluate their proliferation. L929 cells were first cultured in RPMI 1640 medium containing 10% FBS, 1% PS, and subcultured for two generations. Cells in the plate were digested and counted. Then a 2.4 mL of hydrogel was prepared using RPMI 1640 and added to 6-well plates. Cells were added to the hydrogel at a density of 6×10^5 cells/well and cultured in a 37 °C, 5% CO_2 incubator for 3 days. 1 mL of medium was added above the hydrogel to provide adequate nutrition and moisture every 24 h. The morphology and proliferation of cells in the hydrogel were observed at 12 h intervals using an optical microscope. After 3 days, 1 mL of acetic acid solution (3%) was added to the hydrogel. After standing down for 20 min, the solution was fully blown to completely degrade the hydrogel. Cells were recovered by centrifugation and counted. The experiment was repeated 3 times.

Cell viability of L929 cells after the addition of GC, DF-PEG, and the extract of 2.5% CPH was determined by MTT staining. L929 cells were first cultured in 96-well plates at a density of 5×10^3 cells/well. After 24 h incubation, the medium in each well was removed, 100 μL of fresh 3 wt% GC, 1 wt% DF-PEG, the extract of 2.5% CPH were added, respectively, and co-cultivated for another 24 h. Then, 10 μL of MTT dye was added to each well and incubated at 37 °C for 4 h. 100 μL of 10% sodium dodecyl sulfate (SDS) solution was added to each well to dissolve formazan crystals, and then the absorbance was measured by a microplate reader. The absorbance of the dye was measured at 570 nm. Wells containing only cells and medium were used as controls. Each group had 6 multiple holes, and the experiment was repeated 3 times.

2.6. In vitro degradation

The degradation behavior of the hydrogel was investigated by weightlessness. 1 mL of 2.5% CPH was weighed on a precision electronic balance. Then 5 mL of PBS solution was added and the hydrogel was placed in a constant temperature water bath at 37 °C. The sample was taken out at the set time, wiped dry with filter paper and weighed. The experiment was repeated three times.

2.7. MWA protocol and therapy in vivo

Beagle dogs were anesthetized with 5% pentobarbital intravenously (30 mg/kg). After adequate anesthesia, the dog was placed in the supine position, neck posterior flexion followed by endotracheal intubation. Each Beagle dog's neck was shaved. Then the dogs were randomly divided into 3 groups (n = 3). The color doppler ultrasound (CDU) system (SAMSUNG, Korea) was used to locate the thyroid. Ultrasonic imaging was performed on the thyroid gland before the injection of insulator. Under the ultrasonic guidance, a safe and close path was selected, avoiding important structures such as neck blood vessels, trachea, and nerves. The ablation probe and thermometer were punctured separately into the thyroid. The insulator (normal saline, 2.5% CPH, 20% F127) was injected. The uniform distribution of the insulator around the thyroid was examined by CDU. During the MWA of the thyroid, the isolation was always monitored by CDU. All operations were performed by experienced sonographers.

The equipment is a MWA treatment apparatus (KY-2000, Canyon Medical Inc., Nanjing, China). The maximum power of the microwave emission source is 100 W. A 16 G MWA probe with a 3 mm electrode tip at the tip is used. The electrode kit uses normal saline for cooling. The generator power was set to 30 W and each ablation time was maintained for 15 s. The thermometer was used to synchronously perform temperature measurement operations. Thermal ablation was stopped

when the CDU showed that the lesion was completely covered by strong echoes generated from thermal ablation. The entire ablation process was monitored by using CDU in real-time.

During MWA, the CDU was used to record the position of the thermometer and the MWA apparatus was used to record the temperature. After the ablation treatment, the Beagle dog was euthanized and dissected.

2.8. Histology analysis

Hematoxylin-Eosin (H&E) staining was used to evaluate the damage of blood vessels in the neck of Beagle dog. After MWA treatment, the neck blood vessels were removed under deep anesthesia. Then, the blood vessels were incubated in 4% paraformaldehyde for 24 h and fixed immediately before being dehydrated in paraffin embedding. All paraffin Section (4 μm thick) were processed for H&E staining and stained sections were visualized under an optical microscope equipped with a CCD camera.

2.9. In vivo degradation

As an insulator of MWA, the degradation time of CP hydrogel in vivo is a matter of concern. After injecting 2.5% CPH into the neck of Beagle dog, the hydrogel was examined by CDU, the state of the hydrogel was recorded, and the separation distance was measured. To monitor degradation of the hydrogel in vivo, the ultrasonic imaging was performed daily over the subsequent 7 days.

2.10. In vitro heat transfer analysis

A device was built to monitor the heat transfer of different mediums in vitro. Normal saline, 2.5% CPH, 2.5% F127, 16% F127, 20% F127 were added into the cylindrical glass and the heating bar was vertically inserted into the glass with the liquid level at 3/4 of the heating bar. An infrared camera was erected above the device to capture the dynamic heat transfer process of the medium. The power of the heating rod is 100 W and the heating time is 15 s. The heat transfer process was recorded by using an infrared camera during heating.

2.11. Thermal properties analysis

The thermal properties of hydrogels were measured through the transient plane source (TPS) method by using the Hot Disk thermal constant analyzer [34–36]. TPS method is to place a transient plane probe between two samples, ensuring that each plane of the sample faces the probe. The probe is a double helix etched with sheet metal, sandwiched by two thin insulating materials. When a current flows, the temperature of the probe increases, and the resistance changes with time. The probe provides a small constant current that generates heat, and the temperature rise is determined by the change in resistance.

When current passes, the probe temperature starts to increase and the probe resistance over time can be expressed as (1).

$$R(t) = R_0[1 + \alpha \{\Delta T_i + \Delta T_{ave}(\tau)\}] \tag{1}$$

where R_0 is the resistance (i.e., t = 0) before the probe is heated, α is the temperature coefficient of resistivity, ΔT_i is the temperature difference on a thin insulation layer covering both sides of the probe material, and makes the heating disk a convenient sensor. $\Delta T_{ave}(\tau)$ is the other side of the insulation layer facing the side of the heat disk sensor. From Eq. (1), the temperature increase recorded by the sensor can be obtained.

$$\Delta T_i + \Delta T_{ave}(\tau) = \frac{1}{\alpha} \left[\frac{R(t)}{R_0} - 1 \right] \tag{2}$$

Among them, ΔT_i is the measurement value of the "thermal contact" between the sensor and the sample surface. When its value is 0, it means

that the ideal "thermal contact" is achieved by using an electrically insulating sample. ΔT_i becomes a constant after a very short time ΔT_i, which can be estimated as follows:

$$\Delta T_i = \frac{\delta^2}{K_i} \tag{3}$$

where δ is the insulating layer thickness, K_i is the insulating layer thermal diffusion coefficient, both are known. The time-based temperature increase is given by Eq. (4).

$$\Delta T_{ave}(\tau) = \frac{P_0}{\pi^{\frac{3}{2}} \cdot a \cdot} \Lambda \cdot \mathrm{D}(\tau) \tag{4}$$

where P_0 is the total power of the transmitter, a is the radius of the sensor, Λ is the thermal conductivity of the test sample, $D(\tau)$ is a time-dependent Eq. independent of size.

$$\tau = \sqrt{\frac{t}{\Theta}} \tag{5}$$

t is the measured value of the time when the transient recording starts, Θ is the characteristic time, defined as:

$$\Theta = \frac{a^2}{k} \tag{6}$$

where k is the thermal diffusivity of the sample.

Using the recorded temperature rise and the calculation of $D(\tau)$ to get a straight line, the intercept is ΔT_i, the slope is $\frac{P_0}{\pi^{\frac{3}{2}} \cdot a \cdot} \Lambda$, the thermal conductivity can be calculated. The thermal diffusivity can be calculated by fitting a straight line.

The principle that TPS follows is Fourier's law of heat conduction, its mathematical expression is

$$\Phi = -\lambda A \frac{dt}{dx} \tag{7}$$

Φ is the heat flux, λ is the thermal conductivity, that is, Λ in Eq. (4). The relationship between thermal diffusivity and thermal conductivity is

$$k = \frac{\lambda}{\rho c} \tag{8}$$

k is the thermal diffusivity of the sample, ρ is the density of the sample, c is the specific heat capacity of the sample, ρc is the volume specific heat capacity of the sample. After calculating the thermal conductivity and thermal diffusivity by Eq. (4), the volumetric specific heat capacity of the sample is calculated by the Eq. (8). The thermophysical data of the hydrogel can be obtained through the above calculation.

3. Results and discussion

3.1. Preparation and characterization of CP hydrogel

The crosslinker DF-PEG$_{4000}$ was synthesized according to the procedure in the previous article (Fig. S1) [30]. CP hydrogel is formed by the dynamic Schiff base C=N bonds, in which the -NH$_2$ groups of GC link with the CHO groups of DF-PEG$_{4000}$ in saline. The 2.5% CPH was prepared by mixing 3 wt% GC solution and 1 wt% DF-PEG$_{4000}$ solution in a volume ratio of 3:1. After 15 min, gelation of CP hydrogel is achieved (Fig. 1a). A 22-gauge needle was used to evaluate the injectability of the hydrogel. The hydrogel could be easily injected without blockage (Fig. 1b), indicating a good shape-adapting capacity. After injection, 2.5% CPH displayed good self-adaptability (Fig. S2) and self-healing capability (Fig. 1c), where the hydrogel that was cut into two pieces healed as a whole after 20 min without breaking under the action of gravity. Results of rheological analysis showed that the mechanical strength of 2.5% CPH was about 290 Pa (Fig. 1d). Based on the rheological recovery test, the strain amplitude sweep analysis of the hydrogel demonstrated its elastic response (Fig. 1e). When the hydrogel was run under a large-amplitude oscillating force ($\gamma = 1000\%$, frequency = 1.0 Hz), the G' value decreased from 270 Pa to 10 Pa, meaning that the gel's network became loose. However, after the amplitude was reduced ($\gamma = 1\%$, frequency = 1.0 Hz), G' quickly returned to its initial value, indicating the rapid recovery of the internal network. All results supported the self-healing ability of 2.5% CPH. The internal structure of the hydrogel was further observed by SEM (Fig. 1f). The internal porous structure suggested a greatly water content of CP hydrogel.
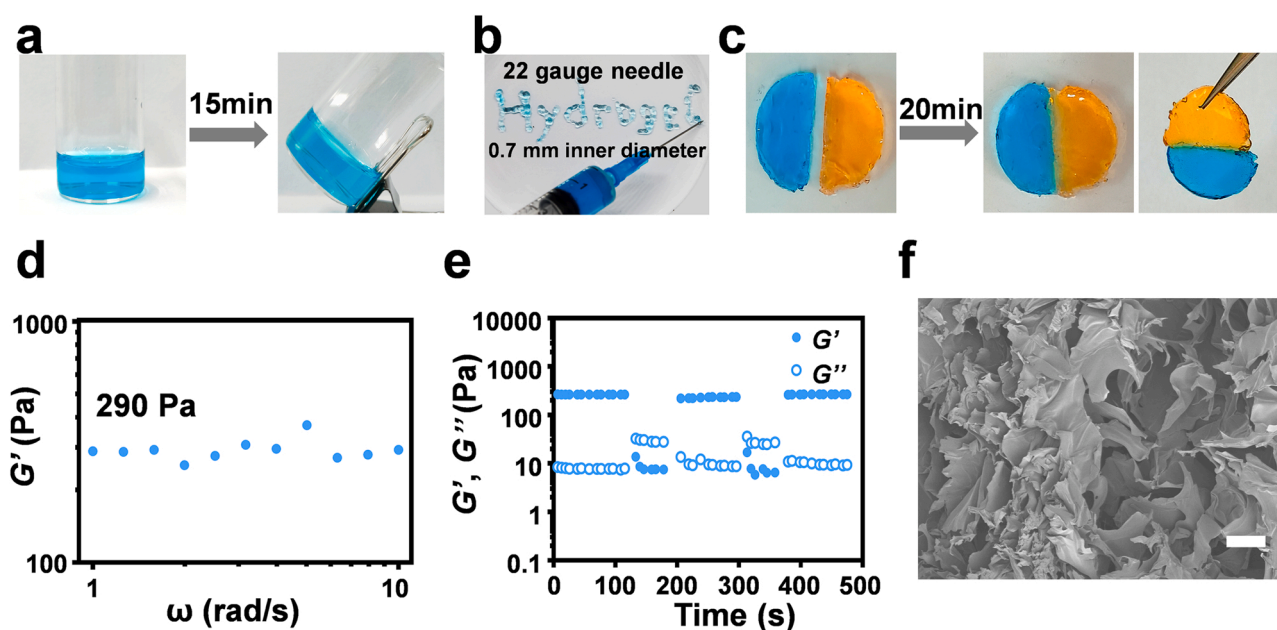
Fig. 1. Characteristics of CP hydrogel. (a) Gelation. (b) Injectability. (c) The self-healing process. (d) Mechanical strength of 2.5% CPH. (e) G' and G'' of 2.5% CPH in step-changing strain measurements. (f) SEM image of 2.5% CPH microstructures. The scale bar is 200 μm.

3.2. MWA protocol in vivo

The CDU was used for thyroid ultrasonography (Fig. 2a). Ultrasonic image Fig. 2b shows that the position of the thyroid gland (region 1) are very close to the neck blood vessels (region 2). If the neck blood vessels are not isolated from the thyroid gland, local high temperature would certainly burn the neck blood vessels and cause bleeding during thyroid ablation.

After injection of normal saline, ultrasonic image showed that the thyroid is successfully isolated from the adjacent tissues (Fig. 2c before). The area was 1.26 cm^2. Notably, upon thyroid ablation, the normal saline had flowed to the adjacent tissue lumen and the isolation area became 0.32 cm^2 (Fig. 2c after). The interval between thyroid and adjacent tissues was shortened, and normal saline no longer had the function of isolation and protection. This is the common problem in clinical use of normal saline as solation fluid, which often leads to a weakened ablation effect, the emergence of postoperative complications, tissue injury and neck vascular injury [13,20–22]. While continuing to inject normal saline at this time would make operation more difficult.

When injected with CPH, ultrasonic image showed that the hydrogel completely isolated the thyroid from the adjacent tissues (Fig. 2d before). The area was 1.32 cm^2. During MWA surgery, the hydrogel did not flow away and had excellent retention *in situ* (Fig. 2d after). As a result, the hydrogel acted as an insulator and protector throughout the procedure, simplifying the operation without being resupplied. After MWA surgery, the neck of the Beagle dog was physiologically dissected (Fig. 2d inset). The hydrogel was completely filled around the thyroid gland, which perfectly blocked the local high temperature produced by MWA and protected the adjacent tissues. This phenomenon demonstrated the effectiveness of a single injection of CPH. Further, the stability of CP hydrogel at saline and high temperatures was investigated
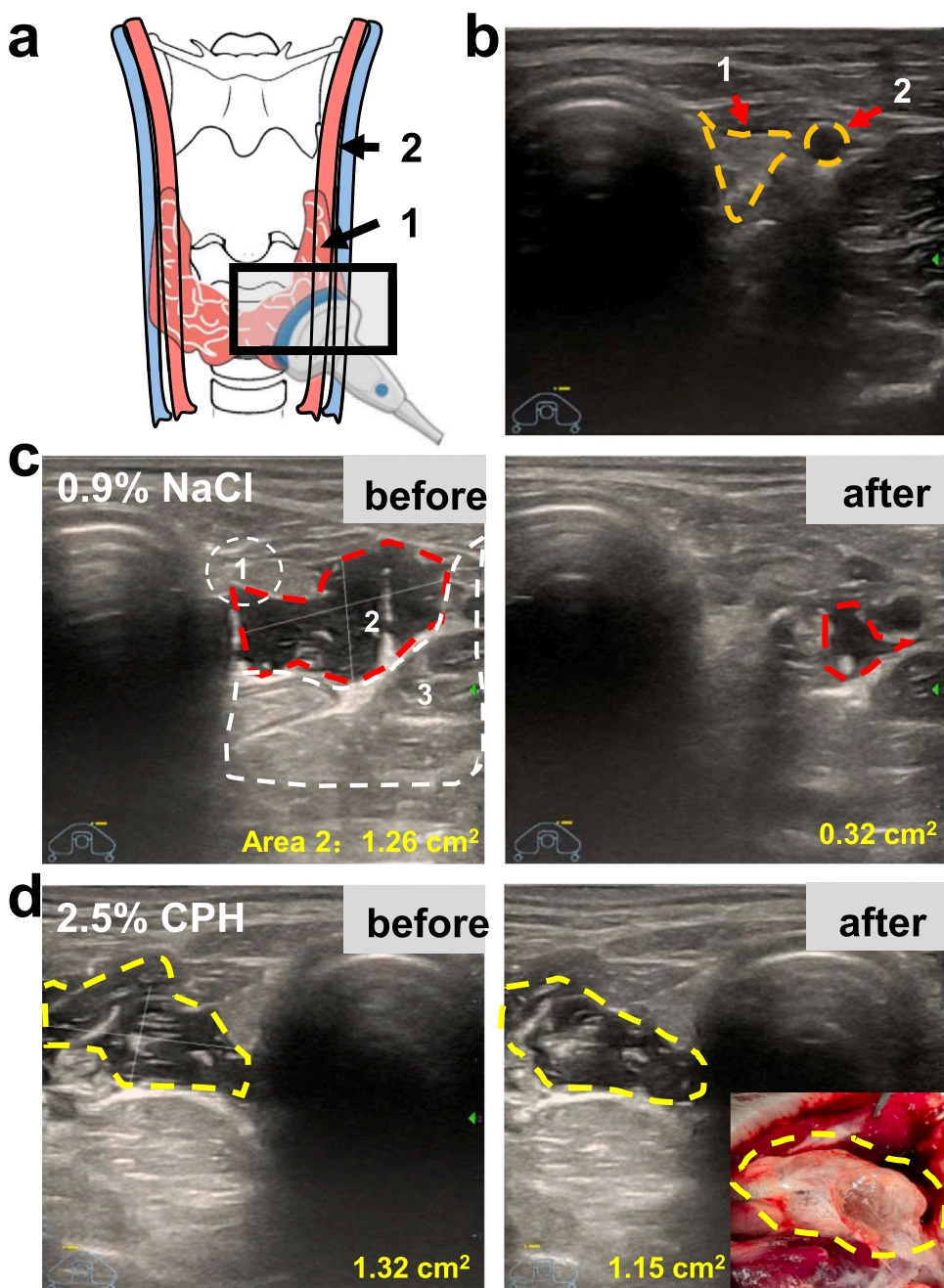
Fig. 2. CDU Ultrasonography of injecting insulators around thyroid gland. (a) Schematic diagram of CDU locating thyroid gland. (b) Ultrasonic image of thyroid gland and carotid artery in Beagle dog. Region 1 is thyroid gland and region 2 is carotid artery. (c, d) Ultrasonic images of injecting normal saline and 2.5% CPH respectively around thyroid gland before and after MWA treatment. Red domain shows the state of normal saline. Yellow domain shows the state of 2.5% CPH. Region 1 is thyroid gland, region 2 is isolation medium, region 3 is adjacent tissues. The bottom right inset is the neck anatomy, showing that the hydrogel is completely wrapped around the thyroid gland.

(Fig. S3). The results indicated that the gel morphology was maintained both in saline and at high temperatures.

3.3. MWA therapy in vivo

MWA therapy of thyroid nodule was performed under the guidance of CDU (Fig. 3a). When normal saline was used as isolation, as shown in Fig. 3b, the temperature near the thyroid gland was 50.5 °C, and the temperature near the blood vessels was 42.7 °C. As we know, the temperature threshold for heat damage to the body is 42 °C [37,38]. At this time, the local high temperature generated by MWA could cause thermal damage to adjacent tissues, in particularly the blood vessels in the neck. When CPH was served as isolation (Fig. 3b), the temperature near the thyroid gland was 41.8 °C, and near the blood vessels was only 37.4 °C, which was close to normal body temperature.

In order to check the continuous change of temperature, the relationships between temperature and distance were recorded. The temperature changing trend of CPH group was obviously lower than that of normal saline group (Fig. 3c). Slower temperature changes would bring less risk of damage. Statistically, the test results exhibited that the neck vascular temperature in the CPH group was much lower than that in the saline group, and even the temperature near the thyroid gland was lower than the temperature threshold (42 °C) for producing thermal injury, while the saline group was higher than the threshold temperature (Fig. 3d). Furthermore, the physiological examination was performed after the surgeries. H&E staining showed no damage of the neck vessels in the CPH group (Fig. 3e). While in the normal saline group, the visual changes of vascular wall and the increase of inflammatory cells were found. This results also indicated that the thermal insulation performance of normal saline was poor.
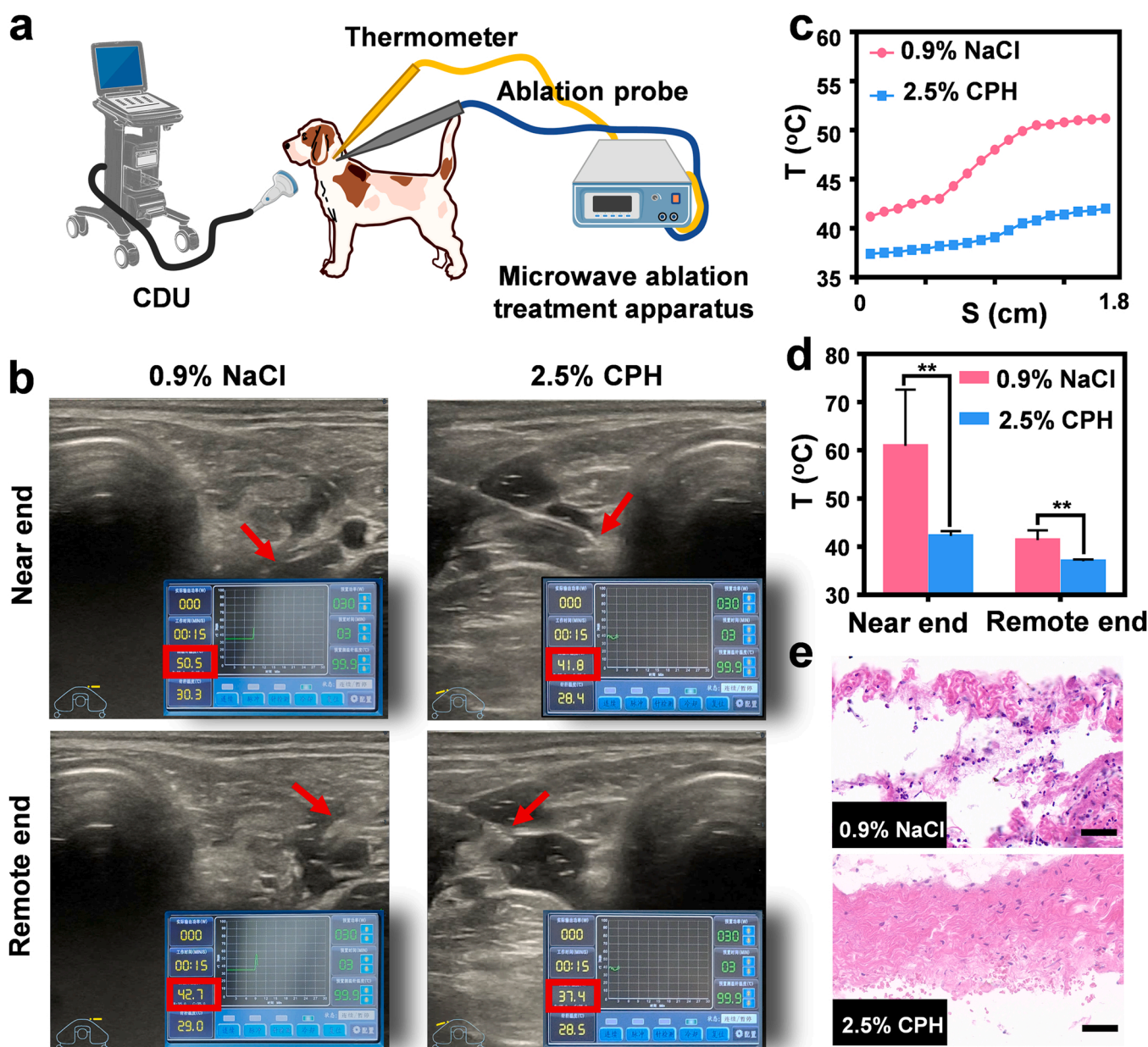
Fig. 3. Thermal shielding performances of MWA therapy *in vivo*. (a) Schematic diagram of MWA therapy of thyroid nodule in Beagle dog model. (b) Ultrasonic images and temperature detection. Normal saline and 2.5% CPH were injected as isolation, respectively. Temperature at the near end and at the remote end were recorded during surgery. (c) The relationship curve between temperature and distance. (d) Statistical analysis of temperature at both ends. The results are expressed as the mean ± SD in all groups (n = 3). **P < 0.01. (e) H&E staining of neck vessels. The scale bar is 50 μm.

In addition, a control group of 20% F127 was also performed. The temperature of the proximal and distal thyroid was lower than 42 °C (Fig. S4). H&E result showed no change in neck vascular wall morphology in the 20% F127 group (Fig. S5). However, compared with the 2.5% CPH group, the gelation time of 20% F127 was shorter, and the hydrogel was often formed in the syringe, which made the injection operation more difficult. We know that if the gelation time is too short, the operation time in clinic will be insufficient. Moreover, the 20% solid content of F127 was far greater than 2.5% of CPH, which may lead to a metabolic burden to the body. But if the solid content is reduced, it is generally difficult for F127 to form a hydrogel state, which may loss the thermal isolation effect. Thus, using the CP hydrogel as an insulator during tumor thermal ablation will greatly improve thermal shielding performance and reduce the risk of postoperative complications.

3.4. Biological safety of CP hydrogel

In order to understand the biosafety and degradation of CP hydrogel in MWA therapy, morphological changes of the hydrogel near thyroid gland were evaluated. After one day of hydrogel injection, the region of CP hydrogel decreased from 3.20 cm^2 to 1.01 cm^2 (Fig. 4a). The hydrogel was mostly degraded after 3 days and completely degraded after 7 days of injection. Due to the low solid content, 97.5% of the hydrogel was normal saline, so no edema was found in situ. According to the quantitative curve of the area of CP hydrogel degradation, the hydrogel was most degraded *in vivo* on day 1, with the largest change in the area, and thereafter decreased slowly (Fig. 4b). Besides, CP hydrogel degraded faster *in vitro* (Fig. S6), which meant that PBS cannot simulate the *in vivo* environment.

Biomedical materials require good biocompatibility. The cytotoxicity of 3 wt% GC, 1 wt% DF-PEG, and 2.5% CPH were tested with L929 cells (Fig. 4c). The results showed that the survival rate of each group was above 85%. Furthermore, L929 cells were 3D cultured in CP hydrogel. The cell morphology and proliferation was checked by optical microscopy. After 3 days, the cell numbers have increased significantly (Fig. 4d), suggesting a good biocompatibility of CP hydrogel.

3.5. Heat insulation analysis

Infrared cameras were used to record the heat transfer of different media by using the device in Fig. 5a, where the heating bar was located in the center of the medium. In the normal saline group, the heat had transferred to the edge at 7 s and the edge temperature was about 51 °C (Fig. 5b). At 15 s, the edge temperature reached 67 °C with a heat transfer area of 100% (Fig. 5c), and a heat transfer distance of 24 mm (Fig. S7). Significantly, the edge temperature remained around 27 °C in the 2.5% CPH group at 15 s (Fig. 5b), with a heat transfer area of only 6.8% (Fig. 5c) and a heat transfer distance of 3.7 mm (Fig. S7). To verify whether only 2.5% CPH can achieve this insulation effect, 2.5% F127 with the same solid content of 2.5% CPH was prepared. 2.5% F127 was a polymer solution and was unable to form a hydrogel. The heat transfer of 2.5% F127 polymer solution was the same as that of normal saline. The explanation may be that despite the presence of polymers in the solution, water molecules are not fixed as in hydrogel, so they are still in irregular thermal motion after heating, and heat transfer is rapid under thermal convection and conduction. This interpretation was verified in the heat transfer of 16% F127. It is partly colloidal and partly solution when the temperature is greater than 37 °C. Therefore, water molecules trapped by the gel network cannot move freely; but the free water molecules continue to transfer heat. As a result, the final heat transfer image appeared a radial shape (Fig. 5b). Due to the poor biocompatibility of 20% F127 (Fig. S8), the high solid content and short operation time were unavoidable drawbacks, despite the fact that 20% F127 showed hydrogel morphology and exhibited a similar thermal insulation effect to 2.5% CPH. Furthermore, the contribution of self-healing to thermal insulation was verified by implementing heat transfer after shearing with 2.5% CPH and 20% F127 (Fig. S9), that is, the self-healing hydrogel can form a uniform and stable medium after injection to
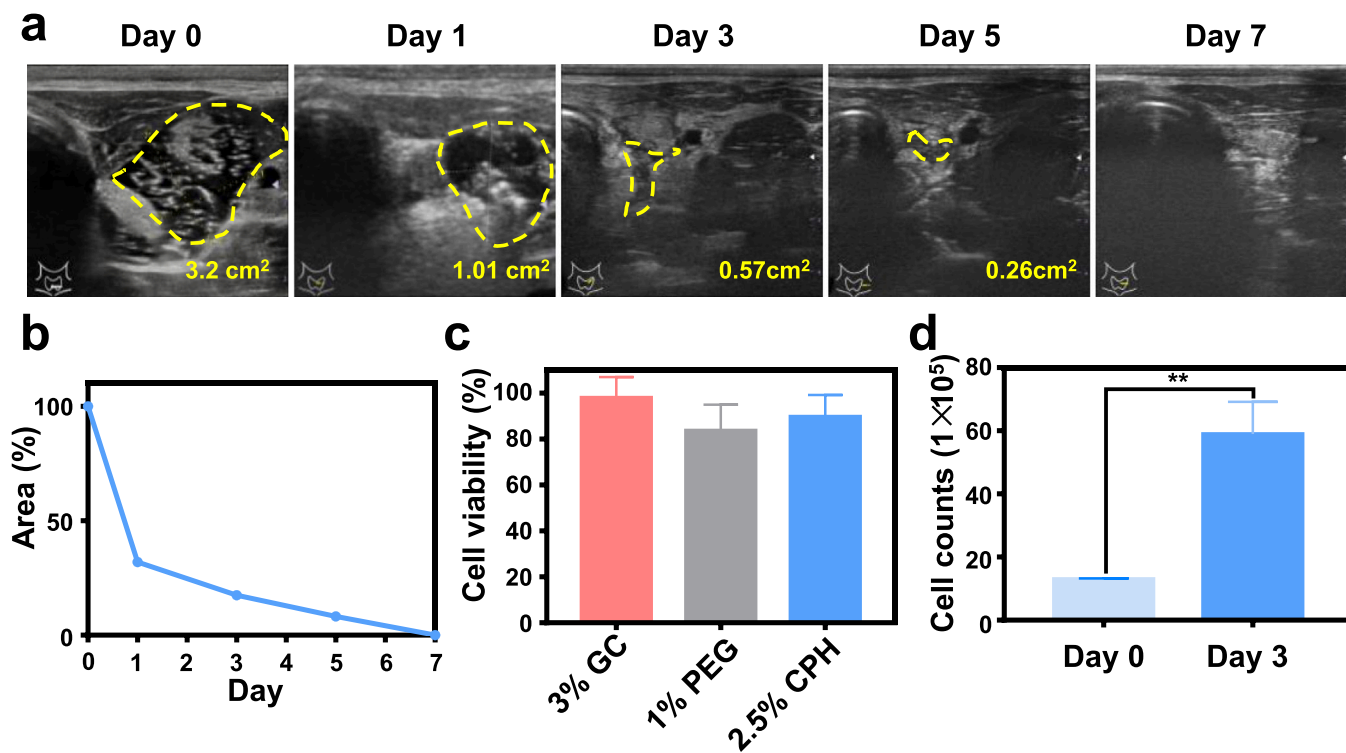
Fig. 4. Biological safety of CP hydrogel. (a) Ultrasonic images of degradation process. (b) Quantificative changes of degradation area. (c) Cytotoxicity of CP hydrogel. The results are expressed as the mean ± SD in all groups (n = 6). (d) The total number of cells after culturing L929 cells in CP hydrogel for 3 days. The results are expressed as the mean ± SD in all groups (n = 3). **P < 0.01.
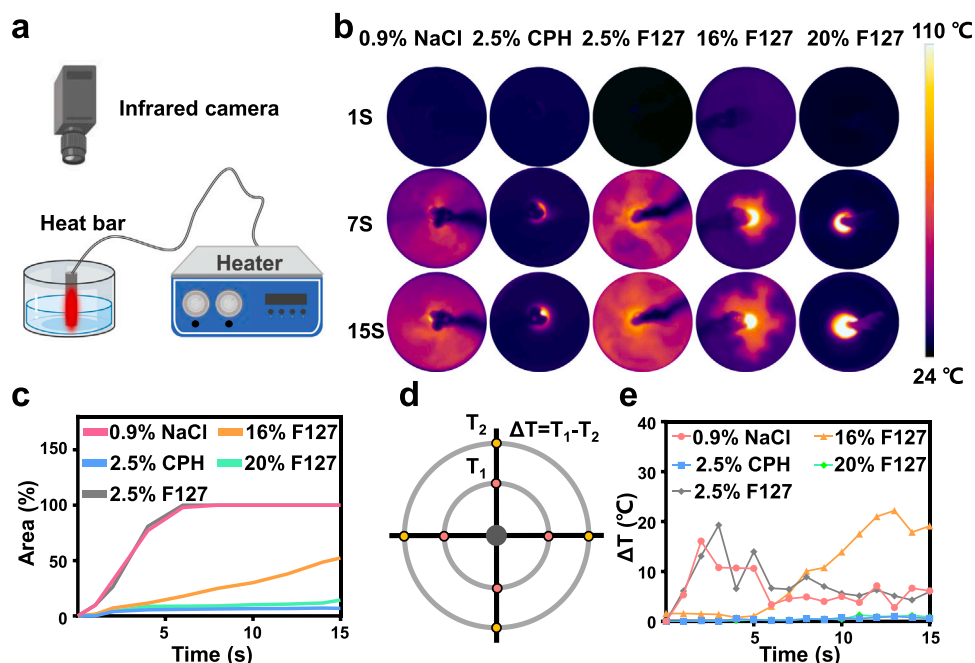
Fig. 5. Heat transfer analysis. (a) Schematic diagram of the heat transfer experimental apparatus. (b) Dynamic infrared images and (c) area change diagram upon heat transfer of different media (normal saline, 2.5% CPH, 2.5% F127, 16% F127 and 20% F127). (d) Schematic representation of the temperature measurement points setting and (e) trend diagram of temperature difference of above infrared images.

achieve a superior thermal shielding effect.

The heat transfer images in Fig. 5b were analyzed in depth, through setting eight measurement points for temperature difference analysis (Fig. 5d). As shown in Fig. 5e, normal saline and 2.5% F127 were solutions, with similar temperature difference trends, both of them reached the highest value in the first 5 s and gradually became gentle thereafter. This was related to heat convection and heat conduction in

solution. If the initial temperature difference is low, the heat mainly depends on heat conduction. Heat is gradually transferred from the center to the edges. With the gradual increase of temperature difference, heat convection will be strengthened. When heat convection is dominant, the solution temperature will become uniform rapidly. The solution in 16% F127 coexisted with hydrogel, where the temperature difference was gradually increased, indicating that the gel state would
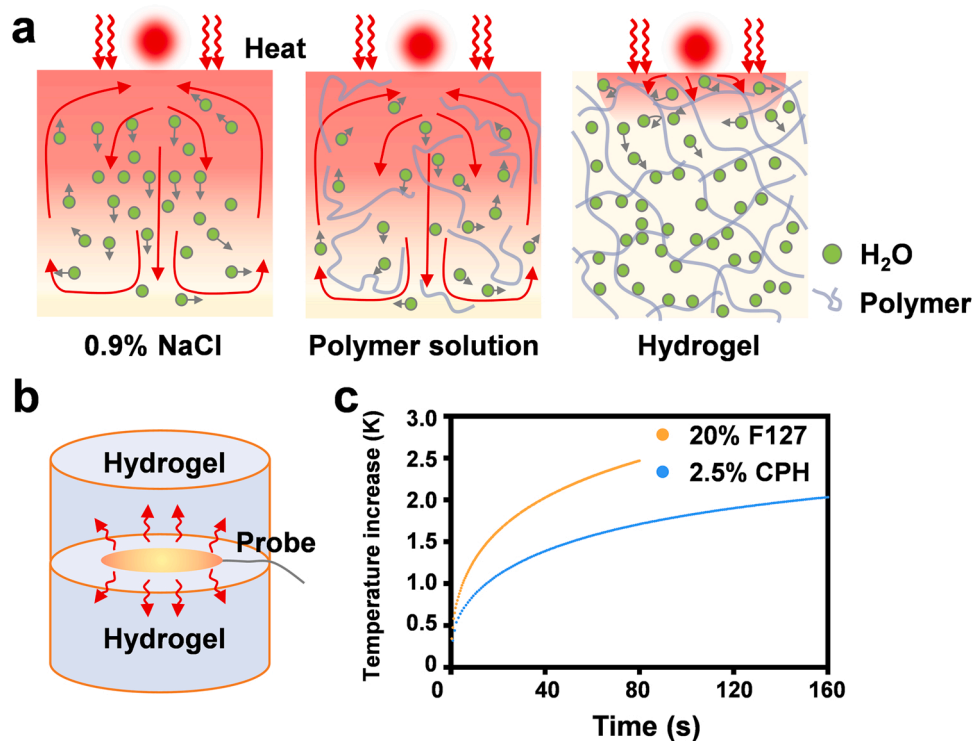
Fig. 6. Heat insulation mechanism of CP hydrogel. (a) Schematic diagram of thermal insulation mechanism of different media (normal saline, polymer solution, hydrogel). (b) Schematic representation of TPS method for measuring hydrogel thermal property. (c) Curves of temperature *versus* time for 2.5% CPH and 20% F127.

hinder heat convection. Both 2.5% CPH and 20% F127 were completely gel states, and the temperature difference of the gel state was close to 0 because the heat didn't transmitted to the measurement point (Fig. 5d), confirming the thermal insulation effect of hydrogels.

3.6. Thermal insulation mechanism

In the basis of above analysis, Fig. 6a shows the thermal insulation mechanism of solution and hydrogel. Water molecules are free in saline and polymer solutions, presenting both heat convection and heat conduction. Convective heat transfer is faster than heat conduction, making the temperature of the solution more uniform [39–41]. But inside the hydrogel, water molecules are bound to the gel backbone [42]. Convective heat transfer in the gel is limited. Thermal conduction depends on the basic properties of the gel, such as thermal conductivity, thermal diffusivity, and heat capacity. Therefore, to further verify the insulation mechanism, the thermal properties of 2.5% CPH and 20% F127 were determined by the TPS method (Fig. 6b). 20% F127 increased by 1.59 K in 80 s, while the 2.5% CPH increased by only 1.26 K within 160 s (Fig. 6c). The heat transfer in 2.5% CPH was distinctly slower and lower than that of 20% F127.

Moreover, Table 1 shows the thermal properties of 2.5% CPH and 20% F127. The thermal conductivity of 20% F127 is 0.5269 W/(m·K), which is lower than 0.6291 W/(m·K) of 2.5% CPH. This result is consistent with basic principle that the greater the water content of the hydrogel is, the higher the thermal conductivity [43,44]. But heat conduction is affected by many factors [45]. The thermal diffusivity refers to drive the uniformity of the temperature inside the object [46]. The thermal diffusivity of 2.5% CPH is $0.1565 \, mm^2/s$, lower than $0.2182 \, mm^2/s$ of 20% F127. However, the specific heat capacity of 2.5% CPH is $4.020 \, MJ/(m^3 \cdot K)$, much higher than $2.414 \, MJ/(m^3 \cdot K)$ of 20% F127. The specific heat capacity refers to the heat absorbed by the system when it rises by 1 K. The lower thermal diffusivity of 2.5% CPH indicates that its internal temperature tends to be uniform more slowly. While the higher specific heat capacity means that it absorbs more heat when the temperature increases by 1 K. Considering above factors, 2.5% CPH had the abilities of poor temperature diffusion, better heat storage, and better heat insulation. Therefore, 2.5% CPH had better thermal shielding performance than 20% F127, even without considering the disadvantage of solid content.

4. Conclusions

In summary, a dynamic self-healing CP hydrogel realized thermal shielding performance in clinical tumor thermal ablation. The dynamic Schiff base enabled the hydrogel to self-heal and self-adapt without external intervention. The injectable property of CP hydrogel simplified clinical practice. *In vivo* and *in vitro* experiments demonstrated that CP hydrogel achieved shape retention *in situ* and heat insulation effect in the process of tumor thermal ablation. The lower thermal diffusivity and higher heat capacity of CP hydrogel endow its better thermal isolation ability. Compared with normal saline and non-healing F127 hydrogel, CP hydrogel with prominent properties including self-healing or self-adapting, injectable and good biocompatibility, is more suitable for heat isolation in clinical thermal ablation, while protecting adjacent tissues from heat damage and reducing related complications. Moreover, 2.5% CPH was non-toxic, while the 20% F127 showed cytotoxicity. Thus, even 20% F127 exhibits the similar thermal insulation efficiency, the low solid content of 2.5% CPH is another advantage by reducing the metabolic burden of the human body. To comprehensive consideration of these factors, CP hydrogel as a protective insulator is a promising thermal management medium in clinical tumor thermal ablation.

CRediT authorship contribution statement

Lifei Huang: Experimental design, Data curation, Writing – original

Table 1
Thermophysical properties of the hydrogels.

Material	2.5% CPH	20% F127
Thermal conductivity (W/(m K))	0.6291	0.5269
Thermal diffusivity (mm^2/s)	0.1565	0.2182
Specific heat ($MJ/(m^3$ K))	4.020	2.414
Temperature increase (K)	1.26	1.59

draft. **Shiyuan Yang:** Investigation, Experimental implementation. **Mingyu Bai:** Supervision, Validation. **Yuxuan Lin:** Supervision, Validation. **Xue Chen:** Formal analysis. **Guofeng Li:** Writing – review & editing. **Li-gang Cui:** Conceptualization, Provision Resources, Funding acquisition. **Xing Wang:** Conceptualization, Provision Resources, Funding acquisition, Writing – review & editing.

Declaration of Competing Interest

The authors declare that they have no known competing financial interests or personal relationships that could have appeared to influence the work reported in this paper.

Acknowledgments

Appendix A. Supplementary material

Supplementary data associated with this article can be found in the online version at doi:10.1016/j.colsurfb.2022.112382.

References

[1] S. Ginzburg, J.J. Tomaszewski, A. Kutikov, Focal ablation therapy for renal cancer in the era of active surveillance and minimally invasive partial nephrectomy, Nat. Rev. Urol. 14 (2017) 669–682.

[2] S.R. Chung, J.H. Baek, Y.J. Choi, J.H. Lee, Longer-term outcomes of radiofrequency ablation for locally recurrent papillary thyroid cancer, Eur. Radiol. 29 (2019) 4897–4903.

[3] K. Yu, B. Liang, Y. Zheng, A. Exner, M. Kolios, T. Xu, D. Guo, X. Cai, Z. Wang, H. Ran, L. Chu, Z. Deng, PMMA-Fe₃O₄ for internal mechanical support and magnetic thermal ablation of bone tumors, Theranostics 9 (2019) 4192–4207.

[4] X. Han, R. Wang, J. Xu, Q. Chen, C. Liang, J. Chen, J. Zhao, J. Chu, Q. Fan, E. Archibong, L. Jiang, C. Wang, Z. Liu, In situ thermal ablation of tumors in combination with nano-adjuvant and immune checkpoint blockade to inhibit cancer metastasis and recurrence, Biomaterials 224 (2019), 119490.

[5] S. Munireddy, S. Katz, P. Somasundar, N.J. Espat, Thermal tumor ablation therapy for colorectal cancer hepatic metastasis, J. Gastrointest. Oncol. 3 (2012) 69–77.

[6] S. Lakhtakia, D. Seo, Endoscopic ultrasonography-guided tumor ablation, Dig. Endosc. 29 (2017) 486–494.

[7] V.M. Ringel-Scaia, N. Beitel-White, M.F. Lorenzo, R.M. Brock, K.E. Huie, S. Coutermarsh-Ott, K. Eden, D.K. McDaniel, S.S. Verbridge, J.H. Rossmeisl, K. J. Oestreich, R.V. Davalos, I.C. Allen, High-frequency irreversible electroporation is an effective tumor ablation strategy that induces immunologic cell death and promotes systemic anti-tumor immunity, eBioMedicine 44 (2019) 112–125.

[8] M. Ahmed, G. Kumar, M. Moussa, Y. Wang, N. Rozenblum, E. Galun, S.N. Goldberg, Hepatic radiofrequency ablation-induced stimulation of distant tumor growth is suppressed by c-Met inhibition, Radiology 279 (2016) 103–117.

[9] Y. Long, E. Xu, Q. Zeng, J. Ju, Q. Huang, P. Liang, R. Zheng, K. Li, Intra-procedural real-time ultrasound fusion imaging improves the therapeutic effect and safety of liver tumor ablation in difficult cases, Am. J. Cancer Res. 10 (2020) 2174–2184.

[10] W. Shady, E.N. Petre, M. Gonen, J.P. Erinjeri, K.T. Brown, A.M. Covey, W. Alago, J. C. Durack, M. Maybody, L.A. Brody, Percutaneous radiofrequency ablation of colorectal cancer liver metastases: factors affecting outcomes-a 10-year experience at a single center, Radiology 278 (2016) 601–611.

[11] M.E. Klapperich, E.J. Abel, T.J. Ziemlewicz, S. Best, M.G. Lubner, S.Y. Nakada, J. L. Hinshaw, C.L. Brace, F.T. Lee Jr., S.A. Wells, Effect of tumor complexity and technique on efficacy and complications after percutaneous microwave ablation of stage T1a renal cell carcinoma: a single-center, retrospective study, Radiology 284 (2017) 272–280.

[12] F. Izzo, V. Granata, R. Grassi, R. Fusco, R. Palaia, P. Delrio, G. Carrafiello, D. Azoulay, A. Petrillo, S.A. Curley, Radiofrequency ablation and microwave ablation in liver tumors: an update, Oncologist 24 (2019) e990–e1005.

[13] R.C. Maduka, C.E. Gibson, A.S. Chiu, R.A. Jean, N. Wills-Johnson, S.A. Azar, K. Oliveira, V. Ahuja, Racial disparities in surgical outcomes for benign thyroid disease, Am. J. Surg. 220 (2020) 1219–1224.

[14] W. Yue, S. Wang, B. Wang, Q. Xu, S. Yu, Z. Yonglin, X. Wang, Ultrasound guided percutaneous microwave ablation of benign thyroid nodules: safety and imaging follow-up in 222 patients, Eur. J. Radiol. 82 (2013) e11–e16.

[15] X. Zhang, Y.H. Ge, P.Y. Ren, J. Liu, G. Chen, Horner syndrome as a complication after thyroid microwave ablation: Case report and brief literature review, Medicine 97 (2018), e11884.

[16] Y. Zhang, M.-B. Zhang, Y.-K. Luo, J. Li, Y. Zhang, J. Tang, Effect of chronic lymphocytic thyroiditis on the efficacy and safety of ultrasound-guided radiofrequency ablation for papillary thyroid microcarcinoma, Cancer Med. 8 (2019) 5450–5458.

[17] D. Aydenizoz, O.T. Selcuk, B. Cekic, E.A. Cetinkaya, A case of vocal cord paralysis after thyroid nodule microwave ablation, Int. Med. 2 (2020) 362–365.

[18] D.T. Ginat, W.E. Saad, Bowel displacement and protection techniques during percutaneous renal tumor thermal ablation, Tech. Vasc. Interv. Radiol. 13 (2010) 66–74.

[19] G.M. Lee, J.Y. You, H.Y. Kim, Y.J. Chai, H.K. Kim, G. Dionigi, R.P. Tufano, Successful radiofrequency ablation strategies for benign thyroid nodules, Endocrine 64 (2019) 316–321.

[20] Y. Korkusuz, D. Groner, N. Raczynski, O. Relin, Y. Kingeter, F. Grunwald, C. Happel, Thermal ablation of thyroid nodules: are radiofrequency ablation, microwave ablation and high intensity focused ultrasound equally safe and effective methods? Eur. Radiol. 28 (2018) 929–935.

[21] C. Kim, J.H. Lee, Y.J. Choi, W.B. Kim, T.Y. Sung, J.H. Baek, Complications encountered in ultrasonography-guided radiofrequency ablation of benign thyroid nodules and recurrent thyroid cancers, Eur. Radiol. 27 (2017) 3128–3137.

[22] B. Feng, P. Liang, Z. Cheng, X. Yu, J. Yu, Z. Han, F. Liu, Ultrasound-guided percutaneous microwave ablation of benign thyroid nodules: experimental and clinical studies, Eur. J. Endocrinol. 166 (2012) 1031–1037.

[23] X.Y. Liu, J. Liu, S.T. Lin, X.H. Zhao, Hydrogel machines, Mater. Today 36 (2020) 102–124.

[24] H. Jiang, Z. Wang, H. Geng, X. Song, H. Zeng, C. Zhi, Highly flexible and self-healable thermal interface material based on boron nitride nanosheets and a dual cross-linked hydrogel, ACS Appl. Mater. Interfaces 9 (2017) 10078–10084.

[25] A.C. Daly, L. Riley, T. Segura, J.A. Burdick, Hydrogel microparticles for biomedical applications, Nat. Rev. Mater. 5 (2020) 20–43.

[26] X. Wang, X. Zhao, T. Lin, H. Guo, Thermo-sensitive hydrogel for preventing bowel injury in percutaneous renal radiofrequency ablation, Int. Urol. Nephrol. 48 (2016) 1593–1600.

[27] Y. Zhang, L. Tao, S. Li, Y. Wei, Synthesis of multiresponsive and dynamic chitosan-based hydrogels for controlled release of bioactive molecules, Biomacromolecules 12 (2011) 2894–2901.

[28] X. Zhou, Y. Li, S. Chen, Y.-N. Fu, S. Wang, G. Li, L. Tao, Y. Wei, X. Wang, J.F. Liang, Dynamic agent of an injectable and self-healing drug-loaded hydrogel for embolization therapy, Colloids Surf. B 172 (2018) 601–607.

[29] T.C. Tseng, L. Tao, F.Y. Hsieh, Y. Wei, I.M. Chiu, S.H. Hsu, An injectable, self-healing hydrogel to repair the central nervous system, Adv. Mater. 27 (2015) 3518–3524.

[30] Y. Li, X. Wang, Y.-N. Fu, Y. Wei, L. Zhao, L. Tao, Self-adapting hydrogel to improve the therapeutic effect in wound-healing, ACS Appl. Mater. Interfaces 10 (2018) 26046–26055.

[31] Y.-N. Fu, Y. Li, B. Deng, Y. Yu, F. Liu, L. Wang, G. Chen, L. Tao, Y. Wei, X. Wang, Spatiotemporally dynamic therapy with shape-adaptive drug-gel for the improvement of tissue regeneration with ordered structure, Bioact. Mater. 8 (2022) 165–176.

[32] Y. Kou, S.Y. Wang, J.P. Luo, K.Y. Sun, J. Zhang, Z.C. Tan, Q. Shi, Thermal analysis and heat capacity study of polyethylene glycol (PEG) phase change materials for thermal energy storage applications, J. Chem. Thermodyn. 128 (2019) 259–274.

[33] S. Karaman, A. Karaipekli, A. Sari, A. Bicer, Polyethylene glycol (PEG)/diatomite composite as a novel form-stable phase change material for thermal energy storage, Sol. Energy Mater. Sol. Cells 95 (2011) 1647–1653.

[34] A.A. Trofimov, J. Atchley, S.S. Shrestha, A.O. Desjarlais, H. Wang, Evaluation of measuring thermal conductivity of isotropic and anisotropic thermally insulating materials by transient plane source (Hot Disk) technique, J. Porous Mater. 27 (2020) 1791–1800.

[35] H. Zhang, Y.M. Li, W.Q. Tao, Efficacy of arsenic trioxide drug-eluting stents in the treatment of coronary heart disease, Int. J. Heat Mass Transf. 108 (2017) 1634–1644.

[36] H. Zhang, Y.M. Li, W.Q. Tao, Effect of radiative heat transfer on determining thermal conductivity of semi-transparent materials using transient plane source method, Appl. Therm. Eng. 114 (2017) 337–345.

[37] Y. Liang, C. Xu, F. Liu, S. Du, G. Li, X. Wang, Eliminating heat injury of zeolite in hemostasis via thermal conductivity of graphene sponge, ACS Appl. Mater. Interfaces 11 (2019) 23848–23857.

[38] G. Power, Z. Moore, T. O'Connor, Measurement of pH, exudate composition and temperature in wound healing: a systematic review, J. Wound Care 26 (2017) 381–397.

[39] Q. Chen, M.R. Wang, N. Pan, Z.Y. Guo, Estrogen-related receptor alpha inverse agonist enhances basal glucose uptake in myotubes through reactive oxygen species, Energy 34 (2009) 1199–1206.

[40] A. Gandomkar, K.E. Gray, Local thermal non-equilibrium in porous media with heat conduction, Int. J. Heat Mass Transf. 124 (2018) 1212–1216.

[41] H.J. Xu, Z.B. Xing, F.Q. Wang, Z.M. Cheng, Review on heat conduction, heat convection, thermal radiation and phase change heat transfer of nanofluids in porous media: fundamentals and applications, Chem. Eng. Sci. 195 (2019) 462–483.

[42] D. Pasqui, M.D. Cagna, R. Barbucci, Polysaccharide-based hydrogels: the key role of water in affecting mechanical properties, Polymers 4 (2012) 1517–1534.

[43] N. Tang, Z. Peng, R. Guo, M. An, X. Chen, X. Li, N. Yang, J. Zang, Thermal transport in soft PAAm hydrogels, Polymers 9 (2017) 688.

[44] S. Xu, S. Cai, Z. Liu, Thermal conductivity of polyacrylamide hydrogels at the nanoscale, ACS Appl. Mater. Interfaces 10 (2018) 36352–36360.

[45] M.U. Sajid, H.M. Ali, Thermal conductivity of hybrid nanofluids: a critical review, Int. J. Heat Mass Transf. 126 (2018) 211–234.

[46] A. Salazar, On thermal diffusivity, Eur. J. Phys. 24 (2003) 351–358.